New Materials, Compounds and Applications
Vol.9, No.3, 2025, pp.570-584
https://doi.org/10.62476/nmca.93570

HIGH EFFICIENCY RED-EMITTING $CaZrTiO_3:Eu^{3+}$ PHOSPHORS FOR WLEDS AND PHOTOCATALYTIC ACTIVITY FOR METHYLENE BLUE AND CRYSTAL VIOLET DYES DEGRADATION

Zahraa T. Abbas[1,2], Dhia A. Hassan[1*], Li Chao[3], Xu Jian[3]

[1]Department of Chemistry, College of Education for Pure Sciences, University of Basrah, Basrah, Iraq
[2]Educational Directorate of Basrah, Ministry of Education, Basrah, Iraq
[3]Lab of New Energy Materials and Devices, School of Physics and Electronic Information Engineering, Henan Polytechnic University, Jiaozuo, China

Abstract. This research investigated the crystal structure, photoluminescence and photocatalytic characteristics of $Ca_{1-x}Zr_{x/2}TiO_3:x/2Eu^{3+}$ phosphors. The phosphors were synthesized using a solution combustion method, with different concentrations of Zr^{4+} and Eu^{3+} dopants to improve their structural and optical properties. The synthesized phosphors' photocatalytic activity has been evaluated through the use of methylene blue (MB) and crystal violet (CV) dyes. X-ray diffraction analysis and scanning electron microscopy were utilized to characterize the phosphors. X-ray diffraction analysis confirmed the perovskite crystal structure of the phosphors, indicating a slight distortion at low doping levels. Photoluminescence spectra exhibited notable emission at 617 nm, corresponding to the red-light band, indicating the potential use of the phosphors in WLEDs. The synthesized phosphors demonstrated significant photocatalytic activity in the degradation of toxic organic dyes under visible light irradiation. The photocatalytic efficiency for CV was 96.01 %, significantly higher than the 70.63% observed for MB. The results indicate the considerable potential of these phosphors for lighting and environmental applications and offer insights into the design of efficient, eco-friendly phosphors for WLEDs and the degradation of harmful pollutants, contributing to sustainable lighting solutions and environmental remediation efforts.

Keywords: *$Ca_{1-x}Zr_xTiO_3:xEu^{3+}$, solution combustion, photoluminescence, LED, dye degradation, photocatalysis.*

Corresponding Author: *Dhia A. Hassan, Department of Chemistry, College of Education for Pure Sciences, University of Basrah, Basrah, Iraq, e-mail: dhia.hassan@uobasrah.edu.iq, dhia_hassan@yahoo.com*

Received: *20 May 2025;* ***Accepted:*** *11 July 2025;* ***Published:*** *4 December 2025.*

1. Introduction

Nowadays, white light-emitting diodes (WLEDs) are thought to be the most widely utilized lighting alternative to fluorescent and incandescent bulbs. Compared to incandescent and fluorescent bulbs, they offer numerous advantages, such as lower negative environmental impact, longer lifespans, safety and higher efficiency (Hassan *et al*., 2016a; Tang *et al*., 2018; Xu *et al*., 2015; Zhang *et al*., 2015). White light is now thought to be most effectively produced by combining a light-emitting diode (LED) chip with phosphor. For example, in commercial devices, $Y_3Al_5O_{12}:Ce^{3+}$ yellow phosphor is paired with a blue GaN LED chip (Muley *et al*., 2022; Xu *et al*., 2016). However, there is a negative aspect to this method, as it has some drawbacks; for example, as a chip ages,

the reduction in red emission can lead to a decline in the color rendering index and instability in correlated color temperature, which requires the discovery and development of new types of red phosphor (Shi *et al*., 2014; Wathook & Hassan, 2024). Furthermore, blue LED chips may emit an excessive amount of blue light. According to biological and medical specialists, too much blue light raises the risk of physiological or psychological problems like depression and sleep disturbances (Yan *et al*., 2017; Yang *et al*., 2013; Zhang & Gong, 2014).

Combining multicolored phosphors with semiconductor chips emitting near-ultraviolet (NUV) light is another method of producing white light. However, due to variations in decay durations and emission color reabsorption, multiphase phosphors lower the luminous efficiency in real-world applications. These challenges could be resolved with a single-composition phosphor that binds to LEDs, serving as a potential solid-state lighting material that emits white light when excited by ultraviolet radiation (Li, 2016; Zhang *et al*., 2014). The typical perovskite structure is calcium titanate ($CaTiO_3$), which has the general formula ABO_3, where A is a cation with a large ionic radius, such as Mg^{2+} or Ca^{2+} and B is a cation with a lower radius, primarily Ti^{4+} or Nb^{5+}. Calcium titanate exhibits superior electrical conductivity (Feng *et al*., 2024; Manjunath & G. Thimmanna, 2016; Nag Bhargavi & Khare, 2015; Peng *et al*., 2010), chemical stability and biocompatibility. These advantages have made $CaTiO_3$ widely used in dielectric resonators, luminous materials and high-frequency dielectric multilayer ceramic (MLC) materials. This type of phosphor can be made through several methods, with the most significant being the sol-gel method (Portia *et al*., 2020; Bharati & Talwar, 2023; Huo *et al*., 2014; Wathook *et al*., 2024), which ensures a pure crystal phase and precise nano-dimensions (Mohammadi & Fray, 2013; Shawky *et al*., 2020); the combustion method, which reduces reaction time (Jegy & Saji, 2024; Vasconcelos *et al*., 2021); the Pechini method, utilizing citric acid and a polyol as chelating agents (Barbieri *et al*., 2023; Delporte *et al*., 2022) and the thermal solution method (Hussain *et al*., 2024; Tuyen *et al*., 2024). Recently, $CaTiO_3:Eu^{3+}$ phosphors have been proposed, capitalizing on these benefits. However, efforts have been made to enhance the emission intensity of $CaTiO_3:Eu^{3+}$ phosphors through charge compensation, crystal distortion and structural replacement. A series of $Ca(Ti_{1-x}Zr_x)O_3:Dy^{3+}$ was prepared to investigate the effect of Zr^{4+} doping concentration on the primary phase and crystal structure of perovskite (Yin *et al*., 2019). Many articles were studied rare-earth elements and transition metals together as activator and co-activator for the hosts (Liu *et al*., 2018; Shimokawa *et al*., 2015; Ueda *et al*., 2023; Yin *et al*., 2019). Additionally, calcium titanate phosphors have various optical applications in the semiconductor industry, modern displays, solar cells and other physical applications (Bai *et al*., 2018; Li *et al*., 2020; Shivram *et al*., 2014).

$CaTiO_3$ is a titanium-based perovskite material utilized as a photocatalyst for environmental remediation applications and has been extensively studied, demonstrating efficacy in degrading aquatic organic pollutants. It utilizes sunlight in the presence of a semiconductor photocatalyst to accelerate the remediation of environmental pollutants and the degradation of highly toxic compounds (Cerón-Urbano *et al*., 2023). UV light and visible commercial light can also be utilized for the excitation of photocatalysis with ease. Photodegradation entails the decomposition of dyes into stable byproducts. It is the most used designation for photocatalytic dye remediation. Photodegradation is considered the complete decomposition into CO_2 and H_2O (Passi & Pal, 2021).

In the present study, the effect of adding or introducing a transition metal Zr^{4+} with a rare earth element Eu^{3+} within the same perovskite $Ca_{1-x}Zr_{x/2}TiO_3:x/2Eu^{3+}$. The Eu^{3+}

ion acts as activator of the host $CaTiO_3$ and the Zr^{4+} ion as a co-activator and both occupy the calcium site in the perovskite structure. It was hypothesized that co-doping Zr^{4+} into the host of $CaTiO_3:Eu^{3+}$ would enhance its luminous properties. We aimed to synthesize and characterize $Ca_{1-x}Zr_{x/2}TiO_3:x/2Eu^{3+}$ phosphors, investigate their crystal structure and photoluminescence for white light-emitting diode applications and evaluate their effectiveness in degrading organic methylene blue and crystal violet dyes pollutants.

2. Materials and methods

2.1. Synthesis of $Ca_{1-x}Zr_{x/2}TiO_3:x/2Eu^{3+}$ phosphors

Different series (x = 0, 0.5, 1,1.5 and 2%) of $Ca_{1-x}Zr_{x/2}TiO_3:x/2Eu^{3+}$ phosphors were synthesized through the solution combustion method. The raw materials were $Ca(NO_3)_2{\cdot}4H_2O$ (Ambition New Materials), $Ti(OC_4H_9)_4$ (Ambition New Materials), $(CH_2OH)_2$ (Sigma Aldrich), $Zr(NO_3)_4{\cdot}5H_2O$ (Ambition New Materials), HNO_3 (CDH 70%), monohydrate citric acid (POCH BASIC) and 4N, Eu_2O_3 powder (Ambition New Materials; 99.9%). In the first step, Eu_2O_3 was dissolved in an acidic HNO_3 solution to obtain an $Eu(NO_3)_3$ aqueous solution. Then $Ca(NO_3)_2{\cdot}4H_2O$ and $Zr(NO_3)_4{\cdot}5H_2O$ were added to the aqueous solution. In the second step, 1 mole of $Ti(OC_4H_9)_4$ was gradually added to 0.005 mole of ethylene glycol in another vessel and the temperature was then increased to 80 °C. Citric acid was added until a clear, transparent, pale-yellow gel was formed. The ion mixture was added slowly until a clear yellow gel was formed. The gel was then sintered at 900 °C for 60 minutes in a high-temperature muffle furnace to yield a white, fluffy powder.

2.2. Determination of the photocatalytic activity of synthesized phosphors

Each photocatalytic experiment was conducted at a constant temperature of 25°C, monitoring the degradation of methylene blue (MB) and crystal violet (CV) under 50 W visible light (10,000 K, AC = 130-265 V). The photocatalytic activities were examined by adding 0.05 g of catalyst particles to a 100 ml beaker containing 25 ml of MB and CV (5 mg/l) aqueous solutions. The suspension was filtered before irradiation and magnetically stirred for several hours in the absence of light to achieve an equilibrium between absorption and desorption. Subsequently, the solutions were stirred while the visible light lamp was on. After the irradiation, the supernatant layer was analyzed for changes in UV-vis absorption bands at 665 nm for MB and 590 nm for CV. The degradation was calculated using the Equation 1 (Hadjltaief *et al*., 2016):

$$\% D = \left(1 - \left(\frac{A_t}{A_0}\right)\right) \times 100 \quad (1)$$

where A_o is the initial concentration and A_t is the absorbance at time *t*.

2.3. Characterization of phosphors

The crystal structure was analyzed using a Rigaku Ultima IV Pro XRD (Japan), equipped with a CuKα radiation source (λ = 0.1540 Å). The analysis was conducted at a scan speed of 20°/min over a 2θ range of 10 to 80°. The morphology of the sample was analyzed using scanning electron microscopy (SEM) with a TESCAN Mira3 (China),

operating in a range of 200-700 nm. The samples were initially mounted on carbon glue and then coated with gold using a sputtering machine. They were subsequently placed in the scanning electron microscope (SEM), where imaging and energy dispersive spectroscopy (EDS) data were collected. The photoluminescence (PL) spectra of all samples were analyzed using an Edinburgh FLS1000 fluorescence spectrophotometer. The photoluminescence excitation (PLE) spectrum was recorded at 617 nm, while the emission PLE spectra were obtained with an excitation wavelength of 466 nm. Hangzhou Rainbow Electronic Co. Ltd. OHSP-350M spectral analyzer, with a 0.3 m integrating sphere, was used to characterize the fabricated WLED device. The maximum wavelength (λ max) and absorption values of the dyes were measured using a JASCO V-730 UV-vis spectrophotometer (Japan), equipped with a xenon (Xe) lamp source.

3. Results and discussion

3.1. XRD analysis

The X-ray diffraction analysis (Figure 1) confirmed the pure phase of the perovskite powder and the presence of a pure crystal structure. It was observed that the prepared phosphors are compatible with the host matrix, which indicated the purity of the obtained phase. It was also observed that the perovskite prepared showed a weak signal at 2θ 27.5° in all the samples except for the low doping percentage of 0.005%, which belongs to rutile TiO_2 (Meroni *et al*., 2017), it indicated the presence of a crystal in a different form.

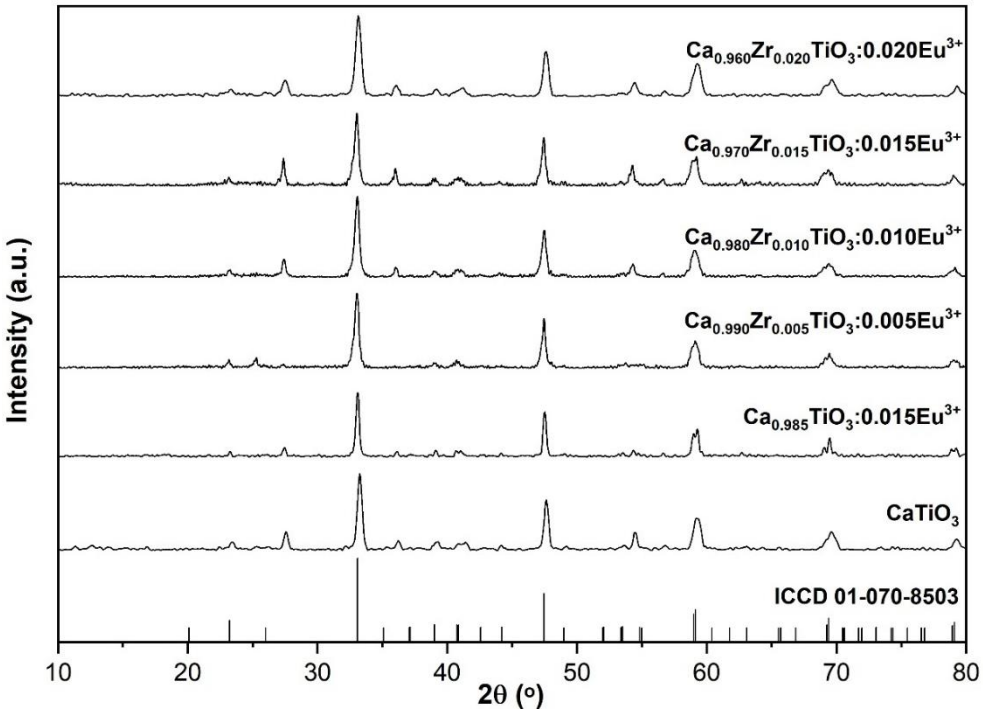

Figure 1. X-ray diffraction pattern of $Ca_{1-x}Zr_{x/2}TiO_3:x/2Eu^{3+}$ phosphors

Alternatively, this could be due to the absence of a center of symmetry in the crystal (Huang *et al*., 2011; Sasaki *et al*., 1987; Wright *et al*., 1992). This indicates that the cooperation between europium and zirconium at concentrations of 0.005 mol assists in obtaining the pure phase. Doping the host of $CaTiO_3$ with Eu^{3+} and Zr^{4+} ions did not alter

the position of the X-ray diffraction peaks, indicating that the doped ions integrated with the host lattice without modifying its crystal structure. All the sample patterns indicated an orthorhombic structure similar to perovskite. The diffraction peaks of the obtained specimens correspond precisely to the typical $CaTiO_3$ diffraction sites and intensities (ICDD-PDF4+: 01-070-8503) of the space group Pbnm (62) with an orthorhombic system and the unit cell parameters were a = 5.39774 Å, b = 5.44661 Å and c = 7.63748 Å and the cell volume is 224.5372 $Å^3$. Crystallite size was determined by using the Scherrer equation:

$$D = \frac{K\lambda}{\beta cos\theta} \quad (2)$$

where *D* is the grain size, *K* is the Scherrer constant = 0.95-0.98, λ is the wavelength of the x-ray source = 0.15405 Å, β is the half-width of the diffraction band (radians) and θ is the Bragg diffraction angle (peak position in radians). It was found that the average crystallite size of the sample $Ca_{0.970}Zr_{0.015}TiO_3:0.015Eu^{3+}$ is 15.587 nm.

3.2. Photoluminescence properties of $Ca_{1-x}Zr_{x/2}TiO_3:x/2Eu^{3+}$ phosphors

The synthesis process greatly influences the attributes of perovskite phosphors; hence, an optimized technique will result in enhanced $Ca_{1-x}TiO_3:xEu^{3+}$ phosphor performance. This study explored the feasibility of combining the sol-gel technique with combination-assisted sintering and using the zirconium as a coactivator along with europium as an activator to produce the $Ca_{1-x}Zr_{x/2}TiO_3:x/2Eu^{3+}$ phosphor to enhance luminous performance. The samples were sintered in a furnace for one hour at 900°C. The luminescence intensity of $CaTiO_3:Eu^{3+}$ is very low compared to when the zirconium ion enters the lattice in the calcium atom sites, indicating a significant improvement in luminescence intensity with the increase in zirconium ion concentration, which comes from the differences between the ionic radius of calcium 0.099 nm and zirconium 0.087 nm.

The emission spectrum recorded at 466 nm in the range of 550-800 nm has four peaks of the produced $Ca_{1-x}Zr_{x/2}TiO_3:x/2Eu^{3+}$ phosphors that were observed at 594 nm, which correspond to $^5D_0 \rightarrow {}^7F_0$ and at 617 nm to $^5D_0 \rightarrow {}^7F_2$ which give the highest intensity. The weak peaks at 653 and 696 nm were observed is belong to $^5D_0 \rightarrow {}^7F_3$ and $^5D_0 \rightarrow {}^7F_4$ transitions, respectively, as shown in Figure 2b. The excitation spectrum monitored at 617 nm in the range of 350-500 nm as shown in Figure 2a has several sharp peaks that were observed at 362, 378, 398, 417 and 466 nm which correspond to the $^7F_0 \rightarrow {}^5D_4$, $^7F_0 \rightarrow {}^5L_4$, $^7F_0 \rightarrow {}^5L_6$, $^7F_0 \rightarrow {}^5D_3$ and $^7F_0 \rightarrow {}^5D_2$ transitions of Eu^{3+} ions, respectively (Wu *et al*., 2012). Figure 3a shows the relation between PL intensity and the concentration of the Eu^{3+} activator and Zr^{4+} coactivator. The highest luminescence was found at 0.015 % of Eu^{3+} and Zr^{4+} because these ions occupy the positions of lowest symmetry, resulting in a significant enhancement in the photoluminescence emission intensity and thereafter it decreases, which indicates the concentration quenching (Hassan *et al*., 2016a; Shi *et al*., 2014). This reduction in emission intensity can be substantiated by the concentration quenching, which is mainly due to the decrease of Eu–Eu distance. As Eu^{3+} concentration increases, the interionic distance between Eu ions decreases, leading to an elevated probability of energy transfer; hence, quenching increases with increasing Eu^{3+} concentration (Girish *et al*., 2019; Kumar *et al*., 2020). It was found in previous reports that the strongest PL intensity of the $CaTiO_3$ doping with Eu^{3+} ions prepared by the sol-gel method followed by annealing at high temperatures was at 0.03 mol of Eu^{3+} (Huong *et al*., 2012). Singh and Manam (2016) found that for the samples made via the chemical

co-precipitation method, the ideal concentration for achieving the maximum PL intensity of $CaTiO_3:Eu^{3+}$ was 0.05 mol, for the samples prepared by the hydrothermal microwave method, it was 0.01 mol of Eu^{3+} (Mazzo *et al*., 2010), while it was found to be 0.16 mol for those prepared by the sol-gel method (Fu *et al*., 2010).

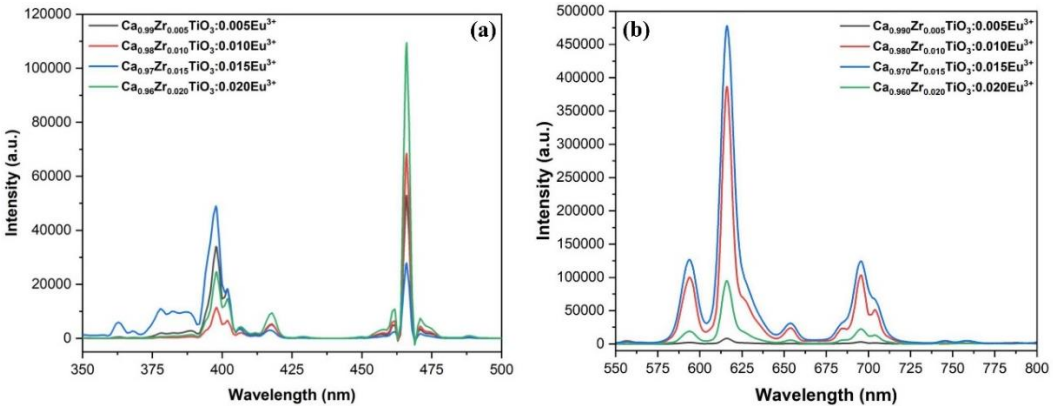

Figure 2. Spectra characteristics of $Ca_{1-x}Zr_{x/2}TiO_3:x/2Eu^{3+}$ phosphors. (a) Excitation at 617 nm; (b) Emission at 466 nm

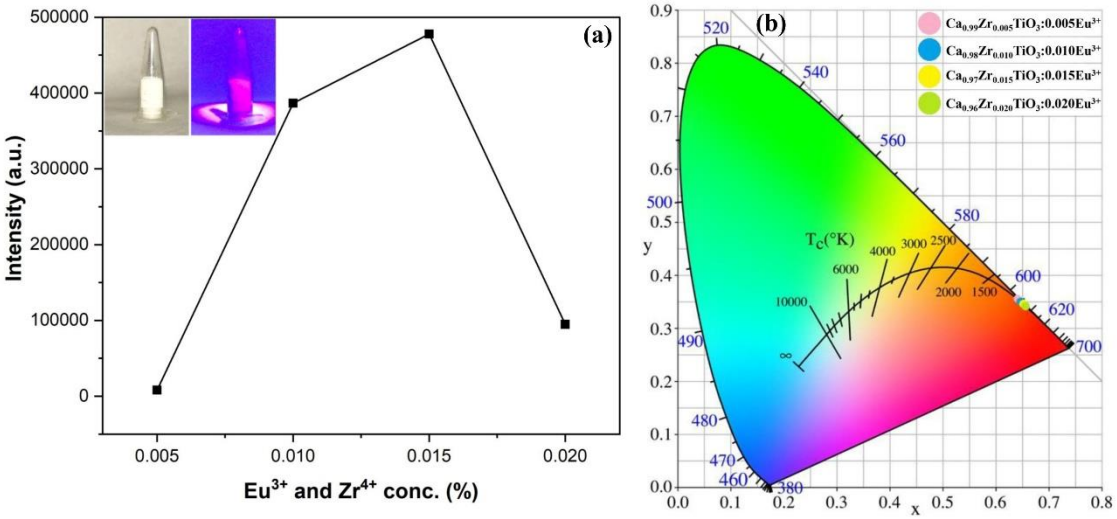

Figure 3. (a) The emission intensity as a function of Eu^{3+} and Zr^{4+}content; (b) the CIE of the prepared phosphor $Ca_{1-x}Zr_{x/2}TiO_3:x/2Eu^{3+}$

Table 1. CIE, CRI and CCT of the prepared phosphors

Sample	CIE		CRI	CCT (K)
	x	y		
$Ca_{0.99}Zr_{0.005}TiO_3:0.005Eu^{3+}$	0.6461	0.3517	44	1053
$Ca_{0.98}Zr_{0.010}TiO_3:0.010Eu^{3+}$	0.6481	0.3502	40	1040
$Ca_{0.97}Zr_{0.015}TiO_3:0.015Eu^{3+}$	0.6540	0.3449	35	1000
$Ca_{0.96}Zr_{0.020}TiO_3:0.020Eu^{3+}$	0.6577	0.3411	34	1000

The CIE, CRI and CCT of the prepared samples are listed in Table 1, all phosphors are placed in the red region. The CIE color coordinates of $Ca_{0.970}Zr_{0.015}TiO_3:0.015Eu^{3+}$ are x = 0.6540 and y = 0.3449 as shown in Figure 3b, the corresponding (x, y) details for the other concentration are listed in the Table 1, according to these values, the synthesized

phosphor can be utilized as a red component in the production of wLEDs and display applications. Therefore, we can mix this red perovskite phosphor with commercial yellow phosphor and apply them on a blue chip to generate white color. The variation and gradient in CIE values in the red region are due to the differing concentrations of Eu^{3+} and Zr^{4+} ions in the $CaTiO_3$ host. The CRI of the samples ranges between 34-44 and the CCT is in the range of candlelight between 1000-1053 K and it decreased with increasing Eu^{3+} and Zr^{4+} concentrations. The inset of Figure 3a shows the prepared red phosphor under UV-light irradiation. The newly developed process enables the preparation of $Ca_{1-x}Zr_{x/2}TiO_3:x/2Eu^{3+}$ red phosphor with excellent luminous performance, suitable for use in wLEDs generation.

3.3. The packaging of the LED

The prepared phosphor $Ca_{0.970}Zr_{0.015}TiO_3:0.015Eu^{3+}$ were combined with a Ce^{3+}-doped yellow YAG phosphor and a SYLGARD 184 PDMS polymer at a 1:2:9 ratio and then applied on the surface of a blue National Star Photoelectric Limited InGaN LED chip measuring 28 x 35 mm via the dispensing coating method. The coated blue LED chip was placed in a vacuum drying oven at 100 °C for 1 h before the temperature was raised to 150°C to bake the chip for 3 h and solidify it. Figure 4a shows the electroluminescence spectrum of the fabricated LED. The 447 nm peak belongs to the electroluminescence of the blue InGaN LED chip and the 579 nm peak to Ce^{3+}-YAG phosphor, while the rest of the spectrum between 590 and 780 nm is for the red phosphor $Ca_{0.97}Zr_{0.015}TiO_3:0.015Eu^{3+}$. The fabricated white LED has a natural white light, as shown in Figure 4b, with a correlated color temperature (CCT) of 4909 K and chromatic coordinates of x = 0.3407 and y = 0.2859 and has a color rendering index (CRI) of 78.7. Consequently, the phosphor prepared by the solution combustion method can effectively generate white light for LED applications.

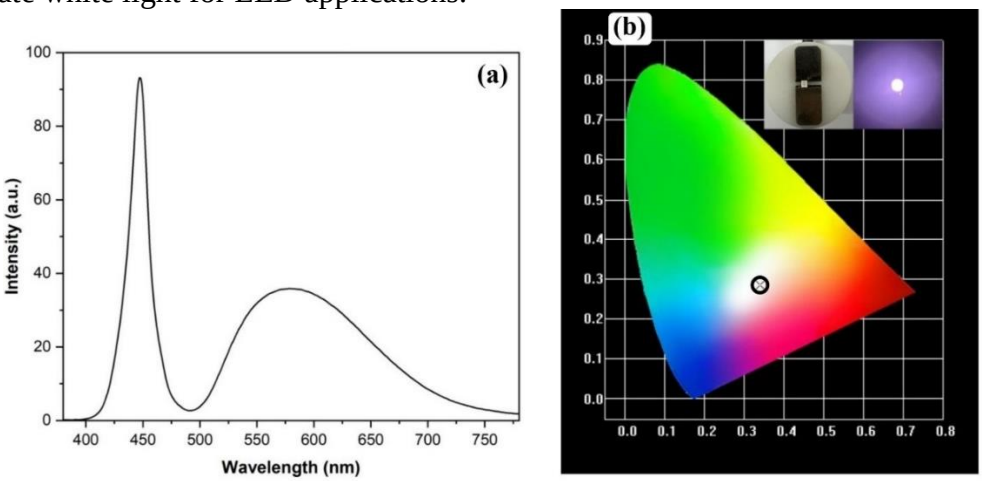

Figure 4. (a) Electroluminescence of InGaN LED chip, red $Ca_{0.970}Zr_{0.015}TiO_3:0.015Eu^{3+}$

3.4. Physical properties of $Ca_{1-x}Zr_{x/2}TiO_3:x/2Eu^{3+}$ phosphors

3.4.1. Determine the maximum wavelength (λ_{max}) of dyes

The results indicated that the prepared phosphor is effective in treating toxic organic dyes and mitigating their harmful impact on the environment. Experiments were conducted to depredate both MB and CV dyes with comparable sunlight after applying.

The Beer-Lambert law and verifying the solutions prepared from the dyes**.** Several analytical tests were conducted to correlate the dyes with the adsorption and treatment processes, including determining the maximum absorption wavelength λ_{max}. The λ_{max} for CV was found to be 590 nm, while it was 665 nm for MB, as shown in Figure 5. (Abbas *et al.*, 2025). The degradation of the CV and MB dyes obeys the Beer-Lambert law, as shown in Figure 6.

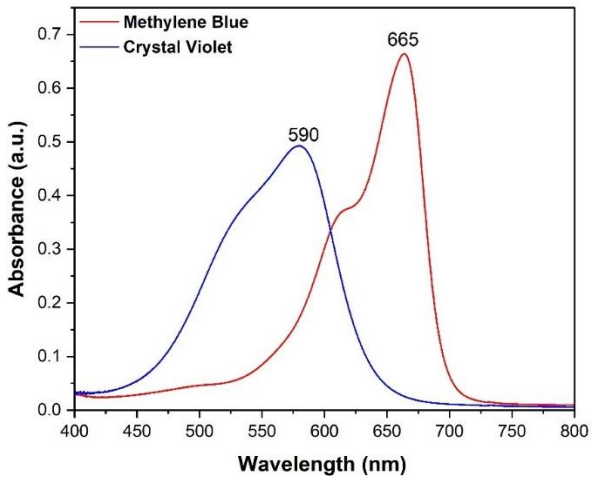

Figure 5. Maximum absorption wavelength (λ_{max}) of crystal violet and methylene blue

3.4.2. The Beer-Lambert law

It is noted from Figure 6 the linear relationship between absorption and concentration, as the R^2 value is close to one, which indicates that the prepared concentrations are very accurate, so it formed a straight line with an excellent value of R^2 and this is consistent with the Beer-Lambert law.

The Beer-Lambert law was evaluated for the dyes; for crystal violet dye, according to the straight-line equation Y = a + b*x, where a = intercept = 0 and b = slope = 0.07598 ± 3.39575E-4; the value of R^2 = 0.99988, which corresponds to the results, is consistent with the Beer-Lambert law as shown in Figure 6a. In methylene blue dye, according to the straight-line equation y = a + b*x, where a = intercept = 0 and b = slope = 0.12433±0.00275; the value of R^2 = 0.99708, which corresponds to the results, is consistent with the Beer-Lambert law, as in Figure 6b (Abbas T *et al.*, 2025).

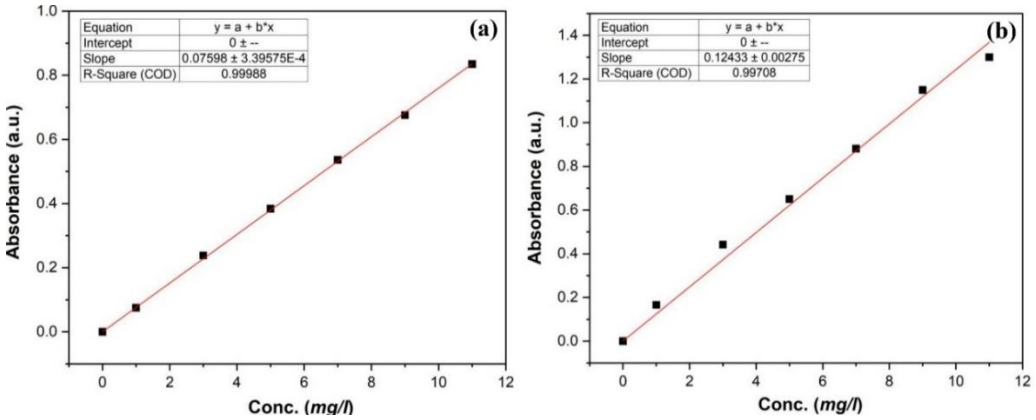

Figure 6. Beer-Lambert law of (a) crystal violet and (b) methylene blue dyes

3.4.3. SEM analysis of the surface

It was also observed that the surface had a clear effect on the dye, as the results showed a decrease in absorption values compared to the control dye. The surface treatment of CV dye under a normal light source simulating sunlight (50 W, 10.000 K, AC = 130-265 V) resulted in a significant reduction in absorption. Due to the exceptionally fine nano-crystalline materials, the phosphor was experimentally studied for its potential to remove or treat toxic organic dyes. It was found that the crystals with an optimal size of 39.89 nm, were produced using the fabrication process. The sol-gel combustion method was used at a sintering temperature of 900°C to produce nanocrystalline phosphor, which were then analyzed using SEM, as showed in Figure 7. The pure perovskite $CaTiO_3$ without activator was shown in Figure 7a. The doping of europium ions as an activator to the $CaTiO_3$ host showed agglomerations and clusters of particles as shown in Figure 7b. However, with the introduction of zirconium ions in Figure 7c $Ca_{0.98}Zr_{0.01}TiO_3$:$0.01Eu^{3+}$ and Figure 7d $Ca_{0.97}Zr_{0.015}TiO_3$:$0.015Eu^{3+}$, the particles became well-distributed and no longer agglomerated or clustered. The images exhibited a nanoscale for the particles of the prepared sample, along with a clear and precise distribution, resulting in a surface morphology characterized by a clear spherical shape with grooves. The distribution was uniform and the grains exhibited no agglomeration, which enhances and is directly proportional to the quality of the photoluminescence and the high percentage of organic dye degradation.

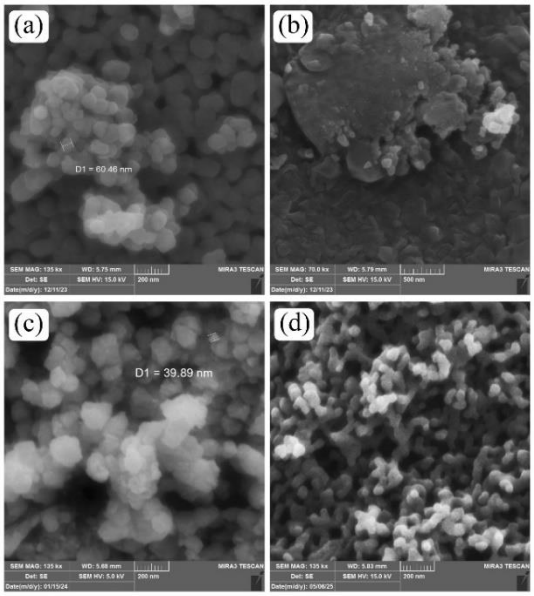

Figure 7. SEM images of (a) $CaTiO_3$, (b) $Ca_{0.99}TiO_3$:$0.01Eu^{3+}$, (c) $Ca_{0.98}Zr_{0.01}TiO_3$:$0.01Eu^{3+}$ and (d) $Ca_{0.97}Zr_{0.015}TiO_3$:$0.015Eu^{3+}$

3.4.4. Degradation of dyes on the surface of perovskite

$CaTiO_3$ is classified as an n-type semiconductor and demonstrates optical absorption within the UV region of the solar spectrum. The mechanism of post-dye degradation is related to both the structural and surface properties of perovskite. Among semiconductor oxide photocatalysts, $CaTiO_3$ is an n-type semiconductor that can absorb

light in the ultraviolet region of the solar spectrum with wavelengths shorter than 450 nm. As is well known, a wide gap exists between the filled valence band (VB) and the empty conduction band (CB) of $CaTiO_3$. When a light source apply with a photon energy (hν) equal to or greater than the band gap energy ($E_g \geq 3.2$ eV) (Cerón-Urbano *et al*., 2023). is illuminated onto $CaTiO_3$, the electrons in the VB are lifted to the CB, thus generating highly energetic electrons (e^-) on the CB and positively charged holes (h^+) on the VB, Only the e^- and h^+ electrons that survive this recombination reach the semiconductor surface and react with dissolved dyes and water molecules adsorbed on the semiconductor surface, respectively, to form superoxide radical anions ($O_2 \cdot^-$) and hydroxyl radicals ($OH^\bullet$). These holes can then oxidize the H_2 molecules to produce powerful hydroxyl radicals, known as OH_2 radicals. These highly reactive radicals ($OH^\bullet$, $O_2 \cdot^-$) can directly attack pollutant molecules adsorbed on the $CaTiO_3$ surface, rapidly producing intermediate compounds. These intermediate compounds are then ultimately converted into green compounds such as CO_2 and H_2O. Therefore, when perovskite is doped with rare earth ions Eu^{3+} and transition metals Zr^{4+}. They are reducing the energy gap (Zhang *et al*., 2023), which allows for the easy transfer of electrons from the valence band to the conduction band, with an increasing ratio of dye degradation, as in the following balanced equations (Passi & Pal, 2021).

$CaTiO_3 + h\nu \rightarrow CaTiO_3(e^-_{CB}) + CaTiO_3(h^+_{VB})$

$CaTiO_3(h^+_{VB}) + H_2O \rightarrow H^+ + OH^\cdot$

$CaTiO_3(e^-_{CB}) + O_2 \rightarrow \dot{O}_2^-$

Polluted (dyes) + $OH\cdot + \dot{O}_2^- \rightarrow$ Intermediate

Intermediate → degradation products + $CO_2 + H_2O$

Regarding the surface shape, the topography of the prepared perovskite greatly encouraged us to apply the adsorption technique as an intermediate step before proceeding with dye degradation. It is clearly noticed from SEM images in Figure 7, the wide and homogeneous spread of the particles and surface free of clumps and aggregates, in addition to the consistency of the spherical particles, especially after adding the zirconium metal to the calcium titanate doped with europium.

To study the degradation of dyes on the surface of perovskite, a reference dye (methylene blue and crystal violet dyes) was prepared at a concentration of 5 mg/L, its absorbance was measured using a UV-Vis spectrometer. The absorbance values were recorded. Next, the dye was adsorbed onto the prepared surface until it reached the optimal adsorption state. Then, the surface of the perovskite $Ca_{0.98}Zr_{0.010}TiO_3:0.010Eu^{3+}$ saturated with dye was placed in a different container with the same dye at a concentration of 5 mg/L. The photocatalytic process was carried out using ordinary light (50 W, 10.000 K, AC 130-265 V). Absorption was recorded for 120 minutes, with 15 min intervals, until equilibrium was reached. It was found that CV provided a high degradation rate of 96.01 % and 70.63 % for MB in the presence of the surface. While the degradation rate of the reference CV was 34.26 % and 28.70 % for MB. The results showed that $Ca_{0.98}Zr_{0.010}TiO_3:0.010Eu^{3+}$ can degrade organic dyes better than the reference dye, which degrades faster when exposed to a light source. The degradation rate was calculated using Equation 1.

The prepared perovskite ceramic $Ca_{0.98}Zr_{0.01}TiO_3:0.01Eu^{3+}$ doped with 0.01 wt.% Eu^{3+} and co-doped with 0.01 wt.% Zr^{4+} was examined for the degradation of MB and CV dyes on its surface. Figure 8a shows the degradation of crystal violet and methylene blue dyes by using the $Ca_{0.98}Zr_{0.01}TiO_3:0.01Eu^{3+}$ phosphor. Figure 8b shows the CV standard control on the left and mixture with phosphor after degradation on the right. Figure 8c

shows the MB standard control on the left and mixture with phosphor after degradation on the right. The results show that the CV dye achieved the highest degradation percentage, reaching 96.01 %, while the same dye without the phosphor had a decomposition percentage of only 34.26 %. The degradation percentage of MB dye was 70.63 %, compared to just 28.70 % for the dye alone, which is significantly low. These results demonstrated that the phosphor can safely and effectively reduce or treat harmful polluting dyes in the environment.

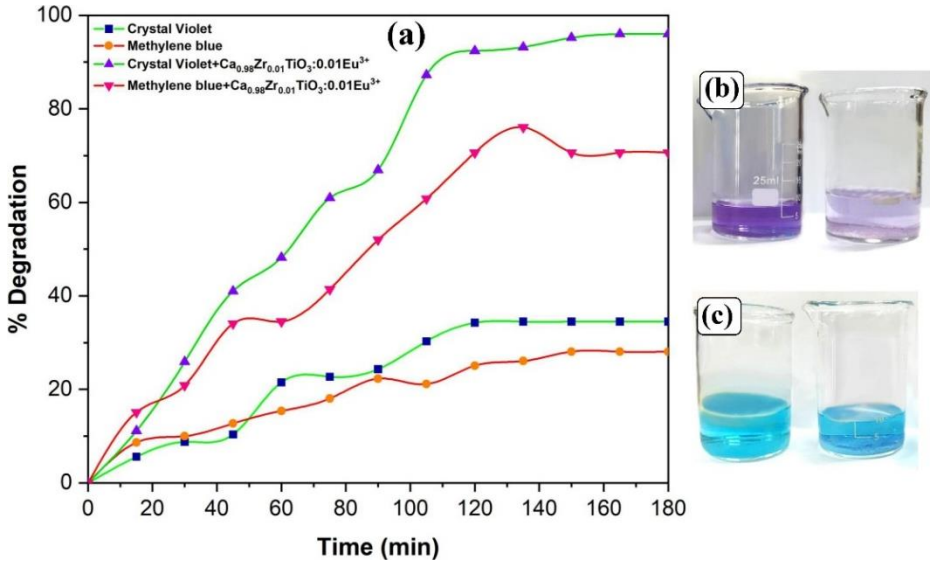

Figure 8. (a) Degradation of CV and MB dyes; (b) CV; (c) MB after and before degradation

4. Conclusions

The series of $Ca_{1-x}Zr_{x/2}TiO_3:x/2Eu^{3+}$ phosphors was synthesized via the solution combustion technique, an efficient and straightforward approach that significantly decreased the calcination time to 60 min. Furthermore, this method guarantees the production of the nanoparticle phosphor with good morphological characteristics and particle dispersion, which improve the luminescence properties. The introduction of zirconium into the host lattice significantly enhances the luminescence intensity of the phosphors. Maximum intensity was found at the concentration of 0.015 % of Eu^{3+} and Zr^{4+}. The fabricated LED is made up of our phosphor $Ca_{0.970}Zr_{0.015}TiO_3:0.015Eu^{3+}$ combined with Ce^{3+}-YAG phosphor and excited with an InGaN LED chip. The fabricated LED produces natural white light, has a CCT of 4909 K and chromatic coordinates in the white region at x = 0.3407 and y = 0.2859 and a CRI = 78.7.

The surface of the fabricated ceramic nanophosphor exhibited significant photocatalytic activity for the degradation of deleterious organic dyes, including methylene blue (MB) and crystal violet (CV), under 50 W irradiation of illumination, with degradation rates of 96.01 % and 70.63 %, respectively. Consequently, it is inferred that the synthesized phosphor offers a sustainable solution for environmental pollution. This research advances the development of luminescent materials for the lighting industry and environmental remediation of damage inflicted upon aquatic ecosystems.

References

Abbas T, Z., A. Hassan, D., Li, C. & Xu, J. (2025). Efficient perovskite $CaTiO_3$: Eu^{3+} co-doped with Mg^{2+} for light emitting diodes and degradation of organic dyes prepared by sol-gel combustion method. *Journal of Sol-Gel Science and Technology*, 115, 808-821. https://doi.org/10.1007/s10971-025-06838-x

Bai, L., Xu, Q. & Cai, Z. (2018). Synthesis of Ag@AgBr/$CaTiO_3$ composite photocatalyst with enhanced visible light photocatalytic activity. *Journal of Materials Science: Materials in Electronics*, *29*(20), 17580-17590. https://doi.org/10.1007/s10854-018-9861-y

Barbieri, F., Dias, L.C., de Oliveira, V.A., Rosso, J.M., Miyahara, R.Y., Santos, B.B.D., … & Freitas, V.F. (2023). On the structural, optical and polarization properties of the incipient ferroelectric $CaTiO_3$ compound. *Ferroelectrics*, *611*(1), 279-286. https://doi.org/10.1080/00150193.2023.2201790

Bharati, A.V., Talwar, B. (2023). Sol-gel assisted optical and structural investigation of Dy^{3+}/Tb^{3+} activated/co-activated $CaTiO_3$ perovskite phosphors by energy transfer mechanism. *Journal of Materials Science: Materials in Electronics*, *34*(35), 2258. https://doi.org/10.1007/s10854-023-11666-2

Cerón-Urbano, L., Aguilar, C.J., Diosa, J.E. & Mosquera-Vargas, E. (2023). Nanoparticles of the perovskite-structure $CaTiO_3$ system: The synthesis, characterization and evaluation of its photocatalytic capacity to degrade emerging pollutants. *Nanomaterials*, *13*(22), 2967. https://doi.org/10.3390/nano13222967

Delporte, M., Cavailles, J., Martin Romo y Morales, M., Bion, N., Nodari, L., Courtois, X., … & Kaper, H. (2022). High-surface-area synthesis of iron-doped $CaTiO_3$ at low temperatures: New insights into oxygen activation, iron states and the impact on methane oxidation. *Inorganic Chemistry*, *61*(39), 15432-15443. https://doi.org/10.1021/acs.inorgchem.2c01966

Feng, J., Mak, C.H., Yu, L., Han, B., Shen, H.H., Santoso, S.P., ... & Hsu, H.Y. (2024). Structural modification strategies, interfacial charge-carrier dynamics and solar energy conversion applications of organic–inorganic halide perovskite photocatalysts. *Small Methods*, *8*(2), 2300429. https://doi.org/10.1002/smtd.202300429

Fu, J., Zhang, Q., Li, Y. & Wang, H. (2010). Highly luminescent red light phosphor $CaTiO^3$:Eu^{3+} under near-ultraviolet excitation. *Journal of Luminescence*, *130*(2), 231-235. https://doi.org/10.1016/j.jlumin.2009.08.012

Girish, K.M., Prashantha, S.C., Naik, R., Nagabhushana, H. & Anantharaju, K.S. (2019). Effect of Bi^{3+} and Li^{+} co-doping on the luminescence properties of Zn_2TiO_4:Eu^{3+} nanophosphor for display applications. *SN Applied Sciences*, *1*(8), 926. https://doi.org/10.1007/s42452-019-0948-8

Hassan, D.A., Xu, J. & Zeng, R. (2016a). Role of synthesis method and α, β-$Sr_{(2-x)}SiO_4$:xEu^{2+} phases on the photoluminescent properties of $Sr_{(1-x)}Si_2O_2N_2$: xEu^{2+} phosphors. *Materials Research Bulletin*, 83, 468-473. https://doi.org/10.1016/j.materresbull.2016.06.024

Hassan, D.A., Xu, J., Chen, Y., Li, L. & Zeng, R. (2016b). Synthesis and photoluminescent properties of $Sr_{(1-x)}Si_2O_2N_2$:xEu^{2+} phosphor prepared by polymer metal complex method for WLEDs applications. *Materials Research Bulletin*, 79, 69-72. https://doi.org/10.1016/j.materresbull.2016.01.048

Huang, G., Dong, W., Fang, L., Zheng, F. & Shen, M. (2011). Effects of Eu-doping site on structural and photoluminescent properties of $CaTiO_3$ particles. *Journal of Advanced Dielectrics*, *1*(2), 215-221. https://doi.org/10.1142/S2010135X11000239

Huo, Y.S., Yang, H., Xian, T., Jiang, J.L., Wei, Z.Q., Li, R.S. & Feng, W.J. (2014). A polyacrylamide gel route to different-sized $CaTiO_3$ nanoparticles and their photocatalytic activity for dye degradation. *Journal of Sol-Gel Science and Technology*, *71*(2), 254-259. https://doi.org/10.1007/s10971-014-3366-9

Huong, D.T.M., Nam, N.H., Vu, L.V. & Long, N.N. (2012). Preparation and optical characterization of Eu^{3+}-doped $CaTiO_3$ perovskite powders. *Journal of Alloys and Compounds*, 537, 54-59. https://doi.org/10.1016/j.jallcom.2012.05.087

Hussain, T., Kousar, R., Younas, K., Saleem, K., Shahzad, A., Munir, T., … & Al-Qahtani, N.H. (2024). Thermoluminescence response of Ce doped $CaTiO_3$ nanophosphor synthesized by hydrothermal method for gamma dosimetry. *Radiochimica Acta*, *112*(12), 999-1006. https://doi.org/10.1515/ract-2024-0282

Jegy, J., Saji, S.K. (2024). Combustion synthesis, rietveld refinement and optical studies of calcium titanate ($CaTiO_3$) perovskites. *AIP Conference Proceedings*, *3149*(1). https://doi.org/10.1063/5.0225041

Kumar, A.N., Jnaneshwara, D.M., Kumar, M.R.A., Basavaraju, N., Ravikumar, C.R., Murthy, H.A., … & Naik, R. (2020). Photoluminescence and electrochemical performances of Eu^{3+} doped $La_{10}Si_6O_{27}$ nanophosphor: Display and electrochemical sensor applications. *Applied Surface Science Advances*, 1, 100026. https://doi.org/10.1016/j.apsadv.2020.100026

Li, G. (2016). Solid state synthesis and luminescence of $NaLa(WO_4)_2$:Dy^{3+} phosphors. *Journal of Materials Science: Materials in Electronics*, *27*(10), 11012-11016. https://doi.org/10.1007/s10854-016-5217-7

Li, S., Li, X., Yang, J., Jiang, Q., Lai, H., Tan, Y., … & Xu, T. (2020). Improvement of photovoltaic performance of perovskite solar cells by interface modification with $CaTiO_3$. *Journal of Power Sources*, 449, 227504. https://doi.org/10.1016/j.jpowsour.2019.227504

Liu, J., Tang, Q., Liu, Z., Zhang, W. & Qiu, K. (2018). Luminescence enhancement of $(Ca_{1-x}M_x)TiO_3$:Dy^{3+} phosphors through partial M (Mg^{2+}/Zn^{2+}) substitution for white-light-emitting diodes. *Ceramics International*, *44*(12), 14774-14780. https://doi.org/10.1016/j.ceramint.2018.05.107

Manjunath, K., G. Thimmanna, C. (2016). Studies on synthesis, characterization and applications of nano $CaTiO_3$ powder. *Current Nanomaterials*, *1*(2), 145-155. https://doi.org/10.2174/2405461501666160805125748

Mazzo, T.M., Moreira, M.L., Pinatti, I.M., Picon, F.C., Leite, E.R., Rosa, I.L.V., … & Longo, E. (2010). $CaTiO_3$:Eu^{3+} obtained by microwave assisted hydrothermal method: A photoluminescent approach. *Optical Materials*, *32*(9), 990-997. https://doi.org/10.1016/j.optmat.2010.01.039

Meroni, D., Porati, L., Demartin, F. & Poelman, D. (2017). Sol-gel synthesis of $CaTiO_3$:Pr^{3+} red phosphors: Tailoring the synthetic parameters for luminescent and afterglow applications. *ACS Omega*, *2*(8), 4972-4981. https://doi.org/10.1021/acsomega.7b00761

Mohammadi, M.R., Fray, D.J. (2013). Synthesis of highly pure nanocrystalline and mesoporous $CaTiO_3$ by a particulate sol-gel route at the low temperature. *Journal of Sol-Gel Science and Technology*, *68*(2), 324-333. https://doi.org/10.1007/s10971-013-3173-8

Muley, A., Dhoble, S.B., Ramesh, P., Yadav, R.S. & Dhoble, S.J. (2022). Recent development of aluminate materials for solid state lighting. *Progress in Solid State Chemistry*, 66, 100347. https://doi.org/10.1016/j.progsolidstchem.2022.100347

Nag Bhargavi, G., Khare, A. (2015). Luminescence studies of perovskite structured titanates: A review. *Optics and Spectroscopy*, *118*(6), 902-917. https://doi.org/10.1134/S0030400X15060156

Passi, M., Pal, B. (2021). A review on $CaTiO_3$ photocatalyst: Activity enhancement methods and photocatalytic applications. *Powder Technology*, 388, 274-304. https://doi.org/10.1016/j.powtec.2021.04.056

Peng, C., Hou, Z., Zhang, C., Li, G., Lian, H., Cheng, Z. & Lin, J. (2010). Synthesis and luminescent properties of $CaTiO_3$:Pr^{3+} microfibers prepared by electrospinning method. *Optics Express*, *18*(7), 7543-7553. https://doi.org/10.1364/OE.18.007543

Portia, S.A.U., Rajkumar, S., Elanthamilan, E., Merlin, J.P. & Ramamoorthy, K.J.I.C.C. (2020). Effect of annealing temperature on structural, optical and visible light photocatalytic performance of $CaTiO_3$ catalysts synthesized by simple sol-gel technique. *Inorganic Chemistry Communications*, 119, 108051. https://doi.org/10.1016/j.inoche.2020.108051

Sasaki, S., Prewitt, C.T., Bass, J.D. & Schulze, W.A. (1987). Orthorhombic perovskite $CaTiO_3$ and $CdTiO_3$: Structure and space group. *Acta Crystallographica Section C*, *43*(9), 1668-1674. https://doi.org/10.1107/S0108270187090620

Shawky, A., Alhaddad, M., Al-Namshah, K.S., Mohamed, R.M. & Awwad, N.S. (2020). Synthesis of Pt-decorated $CaTiO_3$ nanocrystals for efficient photoconversion of nitrobenzene to aniline under visible light. *Journal of Molecular Liquids*, 304, 112704. https://doi.org/10.1016/j.molliq.2020.112704

Shi, Q., Hassan, D.A. & Zeng, R. (2014). Photoluminescence properties of $Na_{1.45}La_{8.55}(SiO_4)_6(F_{0.9}O_{1.1})$: Eu for applications as a reddish orange phosphor. *Functional Materials Letters*, *7*(5), 1450060. https://doi.org/10.1142/S179360471450060X

Shimokawa, Y., Sakaida, S., Iwata, S., Inoue, K., Honda, S. & Iwamoto, Y. (2015). Synthesis and characterization of Eu^{3+} doped $CaZrO_3$-based perovskite type phosphors. part II: PL properties related to the two different dominant Eu^{3+} substitution sites. *Journal of Luminescence*, 157, 113-118. https://doi.org/10.1016/j.jlumin.2014.08.042

Shivram, M., Prashantha, S.C., Nagabhushana, H., Sharma, S.C., Thyagarajan, K., Harikrishna, R. & Nagabhushana, B.M. (2014). $CaTiO_3:Eu^{3+}$ red nanophosphor: Low temperature synthesis and photoluminescence properties. *Spectrochimica Acta Part A: Molecular and Biomolecular Spectroscopy*, 120, 395-400. https://doi.org/10.1016/j.saa.2013.09.114

Singh, D.K., Manam, J. (2016). Structural and photoluminescence studies of red emitting $CaTiO_3:Eu^{3+}$ perovskite nanophosphors for lighting applications. *Journal of Materials Science: Materials in Electronics*, *27*(10), 10371-10381. https://doi.org/10.1007/s10854-016-5123-z

Tang, Q., Qiu, K., Zhang, W., Shen, Y. & Wang, J. (2018). Luminescence enhancement of $Ca_3Sr_3(VO_4)_4:Eu^{3+}$, Sm^{3+} red-emitting phosphor by charge compensation. *Optical Materials*, 75, 258-266. https://doi.org/10.1016/j.optmat.2017.10.040

Tuyen, N.T.T., Tuan, T.Q., Toan, L.V., Tam, L.T. & Pham, V.H. (2024). Synthesis of up-conversion $CaTiO_3:Eu^{3+}$ films on titanium by anodization and hydrothermal method for biomedical applications. *Materials*, *17*(13), 3376. https://doi.org/10.3390/ma17133376

Ueda, K., Ogata, T. & Honma, T. (2023). Effects of codoping on site-dependent Eu^{3+} luminescence in perovskite-type calcium zirconate and hafnate. *Inorganic Chemistry*, *62*(5), 2146-2152. https://doi.org/10.1021/acs.inorgchem.2c03809

Vasconcelos, S.J.T., Silva, M.A.S., de Oliveira, R.G.M., Junior, M.H.B., de Andrade, H.D., Junior, I.S.Q., ... & Sombra, A.S.B. (2021). High thermal stability and colossal permittivity of novel solid solution $LaFeO_3/CaTiO_3$. *Materials Chemistry and Physics*, 257, 123239. https://doi.org/10.1016/j.matchemphys.2020.123239

Wathook, B., Hassan, D.A. (2024). Modified sol-gel method of synthesising a Mn^{4+}-doped Mg_2TiO_4: A red phosphor for improved LED performance. *Annales de Chimie: Science des Materiaux*, *48*(1), 11-16. https://doi.org/10.18280/acsm.480102

Wathook, B., Hassan, D.A., Pang, S. & Jian, X. (2024). Phase transformation and photoluminescence properties of $MgTiO_3:Mn^{4+}$ synthesis by modified sol-gel method. *Chemistry Africa*, *7*(3), 1639-1648. https://doi.org/10.1007/s42250-023-00845-7

Wright, K., Price, G.D. & Poirier, J.P. (1992). High-temperature creep of the perovskites $CaTiO_3$ and $NaNbO_3$. *Physics of the Earth and Planetary Interiors*, *74*(1), 9-22. https://doi.org/10.1016/0031-9201(92)90064-3

Wu, Y.F., Nien, Y.T., Wang, Y.J. & Chen, I.G. (2012). Enhancement of photoluminescence and color purity of $CaTiO_3$:Eu: Phosphor by doping. *Journal of the American Ceramic Society*, *95*(4), 1360-1366. https://doi.org/10.1111/j.1551-2916.2011.04967.x

Xu, J., Hassan, D.A., Zeng, R. & Peng, D. (2015). $Sr_{1.98}Eu_{0.02}SiO_4$ luminescence whisker based on vapor-phase deposition: Facile synthesis, uniform morphology and enhanced luminescence properties. *Materials Research Bulletin*, 71, 106-110. https://doi.org/10.1016/j.materresbull.2015.07.007

Xu, J., Hassan, D.A., Zeng, R.J. & Peng, D.L. (2016). $Lu_3Al_5O_{12}$:Ce@SiO_2 phosphor-in-glass: Its facile synthesis, reduced thermal/chemical degradation and application in high-power white

LEDs. *Journal of the European Ceramic Society*, *36*(8), 2017-2025. https://doi.org/10.1016/j.jeurceramsoc.2016.01.007

Yan, C., Liu, Z., Zhuang, W., Liu, R., Xing, X., Liu, Y., … & Ma, X. (2017). $YScSi_4N_6C:Ce^{3+}$ - a broad cyan-emitting phosphor to weaken the cyan cavity in full-spectrum white light-emitting diodes. *Inorganic Chemistry*, *56*(18), 11087-11095. https://doi.org/10.1021/acs.inorgchem.7b01408

Yang, P., Yu, X., Xu, X., Jiang, T., Yu, H., Zhou, D., … & Qiu, J. (2013). Single-phased $CaAl_2Si_2O_8:Tm^{3+}$, Dy^{3+} white-light phosphors under ultraviolet excitation. *Journal of Solid State Chemistry*, 202, 143-148. https://doi.org/10.1016/j.jssc.2013.03.017

Yin, Q., Qiu, K., Zhang, W., Chen, X., Zhang, P., Tang, Q. & Chen, M. (2019). Crystal structure and luminescence properties of $CaTiO_3:Dy^{3+}$ phosphor co-doped with Zr^{4+}. *Optical Materials*, 98, 109446. https://doi.org/10.1016/j.optmat.2019.109446

Zhang, J., Fan, Y., Chen, Z., Wang, J., Zhao, P. & Hao, B. (2015). Enhancing the photoluminescence intensity of $CaTiO_3:Eu^{3+}$ red phosphors with magnesium. *Journal of Rare Earths*, *33*(10), 1036-1039. https://doi.org/10.1016/S1002-0721(14)60523-8

Zhang, Q., Wang, Y., Jia, Y., Yan, W., Li, Q., Zhou, J. & Wu, K. (2023). Engineering the electronic structure towards visible lights photocatalysis of $CaTiO_3$ perovskites by cation (La/Ce)-anion (N/S) co-doping: A first-principles study. *Molecules*, *28*(20), 7134. https://doi.org/10.3390/molecules28207134

Zhang, X., Gong, M. (2014). Single-phased white-light-emitting $NaCaBO_3:Ce^{3+},Tb^{3+},Mn^{2+}$ phosphors for LED applications. *Dalton Transactions*, *43*(6), 2465-2472. https://doi.org/10.1039/C3DT52328D

Zhang, Z.W., Song, A.J., Ma, M.Z., Zhang, X.Y., Yue, Y. & Liu, R.P. (2014). A novel white emission in $Ca_8MgBi(PO_4)_7:Dy^{3+}$ single-phase full-color phosphor. *Journal of Alloys and Compounds*, 601, 231-233. https://doi.org/10.1016/j.jallcom.2014.02.165